Research Report

Relationship between the Interfacial Roughness and the Giant Magnetoresistance in Co/Cu Superlattices

Motofumi Suzuki, Takeshi Ohwaki, Yasunori Taga

Co/Cu人工格子における界面ラフネスと巨大磁気抵抗効果の関係

鈴木基史，大脇健史，多賀康訓

Abstract

The relationship between the interfacial roughness and the giant magnetoresistance (GMR) in Co/Cu superlattices has been studied. The results have been understood with an *s*-*d* scattering model on the assumption that *d* states are bound in magnetic layers. The GMR in Co/Cu superlattices mainly comes from the spin-dependent *s*-*d* scattering in the Co layers, and the interfacial scattering is less spin-dependent than bulk scattering. This is because of the attenuation of the wave function of *d* states at interfaces.

要　旨

Co/Cu人工格子の巨大磁気抵抗効果 (GMR) を界面ラフネスとの関係に着目して研究した。実験結果は，*d*状態が磁性層内に束縛されていると仮定した*s*-*d*散乱モデルで良く理解できる。すなわち，Co/Cu人工格子のGMRは，主にCo層内におけるスピンに依存した*s*-*d*散乱によって生じており，界面における電子散乱のスピン依存は層内散乱のそれに比べて小さい。これは，*d*状態の波動関数が界面で減衰しているためであると考えられる。

Keywords　Co/Cu, Superlattice, Giant magnetoresistance, Interfacial roughness

1. Introduction

A great number of attempts have been made to clarify the origin of the giant magnetoresistance (GMR) observed in various magnetic multilayers[1-3]. Most of them have focused on the spin-dependent scattering of conduction electrons. Some theoretical studies attribute the GMR to the spin-dependent potential at interfaces[4-6]. In these theories, interfacial roughness is required as the scattering center. The strong spin-dependent scattering also comes from the spin-split density-of-states (SSDOS) for majority- and minority-spin *d* bands in the magnetic layers and occurs both in the bulk and at the interfaces[7,8].

On the other hand, many experimental studies deal with the correlation between the GMR and the interfacial roughness to understand the role of interfaces[9-14]. For Fe/Cr superlattices[9,10], the enhancement of both the magnitude and temperature dependence of the GMR due to interfacial roughness has been reported, so that the origin of the GMR in Fe/Cr is attributed to the interfacial scattering[5]. However, for transition metal (*TM*)/Cu superlattices, no one has reported that the interfacial roughness enhances the GMR[11-14]. Nevertheless, the importance of interfacial scattering has been pointed out indirectly in studies on the layer thickness dependence of the GMR[15,16]. The mechanism of the GMR in *TM*/Cu superlattices still remains unclear.

This lack of understanding lies in the difficulty of quantitatively understanding the relationship between the interfacial structure and the transport properties since the interfacial structure is difficult to control and analyze. In this paper, we report the structure and the GMR of Co/Cu superlattices with well controlled interfacial roughness. The results suggest that the GMR in Co/Cu superlattices mainly comes from the spin-dependent *s-d* scattering in the Co layers.

2. Experiment

2.1 Sample preparation

The Co/Cu superlattices were deposited on surface oxidized Si substrates in a magnetron sputtering system with a base pressure of 2×10^{-7} Torr. After deposition of an Fe buffer layer with a thickness of 5.0 nm, 16 Co/Cu bilayers were grown at room temperature in an Ar pressure of 3×10^{-3} Torr at a deposition rate of 0.2 - 0.3 nm/s. Interfaces between Co and Cu layers were modified by codeposition, which was performed with a computer controlled shutter system. The nominal thickness of the codeposited region t_{mix} was estimated from the deposition rate, and the chemical composition of Co and Cu in the mixed region was to be about 40 and 60 at.%, respectively. The amount of Co and Cu in each bilayer was kept constant at 1.0 and 2.2 nm for pure Co and Cu. The nominal structure of samples was as follows: substrate/ Fe(5.0)/ Cu($2.2-t_{\mathrm{mix}}/2$)/ CoCu(t_{mix})/ [Co($1.0-t_{\mathrm{mix}}$)/ CoCu(t_{mix})/ Cu($2.2-t_{\mathrm{mix}}$)/ CoCu(t_{mix})]$_{15}$/ Co($1.0-t_{\mathrm{mix}}$)/ Cu($2.2-t_{\mathrm{mix}}/2$), where the values in the parentheses are the thickness of layers in the unit of nm. This structure corresponds to the second peak of oscillatory properties of GMR and the antiferromagnetic coupling between adjacent Co layers.

2.2 Structural Analysis

Using a conventional powder diffractometer, high and low angle XRD measurements were performed in a symmetrical reflection($\theta-2\theta$) geometry to characterize the crystallographic structure and the periodicity of superlattices. The divergence of the incident Co $K\alpha$ radiation ($\lambda = 0.179$nm) was 1˚ for high angle XRD and 1/6˚ for low angle XRD. The scattered x-ray was detected with a proportional counter, after the Co $K\beta$ radiation was eliminated with a graphite monochromator.

NMR experiments were carried out in zero field at liquid helium temperature. Each sample was divided into rectangular pieces of 10×20 mm^2. Ten of them were stacked up and were fitted into an exciting coil. Thus, the rf field was applied parallel to the film plane. Using a variable frequency spin-echo apparatus, the distribution of the hyperfine field of ^{59}Co was measured in a frequency range of 120 - 240 MHz. The pulse width and the separation of two rf pulses were kept at constant values of 1.2 μs and 15 μs, respectively. In order to calibrate the frequency dependence of the measurement system, we measured the reference signal together with the spin echo signal. Moreover, we correct the ω^2 dependence of the spin-echo signal to obtain the number of atoms which resonate at a particular frequency[17].

2.3 Measurement of GMR

The in-plane magnetoresistance (MR) was measured with a standard dc four-terminal geometry as a function of the temperature in the range $2 \leq T \leq 300$ K. The dimension of the samples for the measurement was 2×15 mm^2, and the current used was 1 mA. This confirms that the resolution of the measured resistance is better than $10^{-3}\Omega$. In order to minimize the error due to the thermoelectric power in the measurement circuit, we averaged two sequential measurements with different polarities of the current. This sequence was repeated more than 50 times keeping the temperature constant for 10 min, and the collected data were averaged. The standard deviation for the data was smaller than the order of $10^{-4}\Omega$. The resistance-to-resistivity conversion was performed by scaling using the resistivity measured with samples at 300 K large enough to obtain an accuracy of $10^{-2}\mu\Omega$cm.

The magnetization was also measured with a superconducting quantum interface device (SQUID) magnetometer.

3. Results

3.1 Structure of Co/Cu Superlattices[18]

Fig. 1 shows a typical high angle XRD pattern for the samples. Three peaks for fcc Co/Cu are observed. Comparing with the relative intensity of powder diffraction of fcc crystals, our samples show a strong tendency to (110) textured structure. Contrary to the most of sputtered Co/Cu superlattices reported by other workers[2,3], (110) preferred orientation of our samples is characteristic, and is likely to be closely related to the structure of Fe buffer layer[19]. The diffraction patters of samples with different t_{mix} cannot be distinguished from each other. Thus, the crystallographic structures of present samples are independent of t_{mix}, while those of the samples prepared on glass substrates depend on t_{mix} as we reported previously[14].

Low angle XRD patterns are also independent of t_{mix} as indicated in **Fig. 2**. For all the samples different in t_{mix}, Bragg peaks due to the artificial period and Kiessig

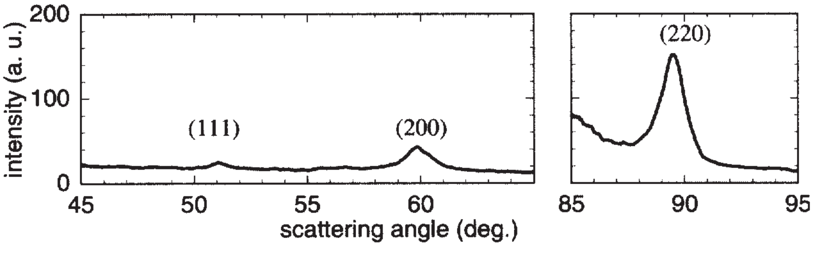

Fig. 1 High angle x-ray diffraction pattern for the sample of $t_{\mathrm{mix}} = 0$ nm[18]. Samples of $t_{\mathrm{mix}} \neq 0$ nm show almost the same diffraction pattern.

fringes are clearly visible. Since the superlattice period is kept constant, these peaks appear at almost the same position. It is remarkable that no significant differences in the amplitude of peaks can be observed between samples. Comparing these results with the calculated diffraction patterns[18], the thickness fluctuation of each layer was less than 0.1 nm for all samples independently of t_{mix}.

In contrast to the XRD, the NMR is sensitive to the atomic short-range order (ASRO). **Fig. 3** shows the frequency spectra of spin-echo intensity of ^{59}Co in the sample of various t_{mix}. The main peak observed around 210 MHz is attributed to the signal from the fcc Co atoms with 12 nearest neighbor Co atoms, while the resonance frequency is slightly lower than that for bulk Co of 217 MHz. Since no significant signal was observed on the higher frequency side of the main peak, the amount of the hcp Co is negligible. There exists a wide distribution of the hyperfine field in the lower frequency region of the main peak down to 120 MHz. The tail at the frequency lower than that of main peak is due to the Co atoms near interfaces. Please note that the intensity of tail increase with t_{mix}. This indicates that the

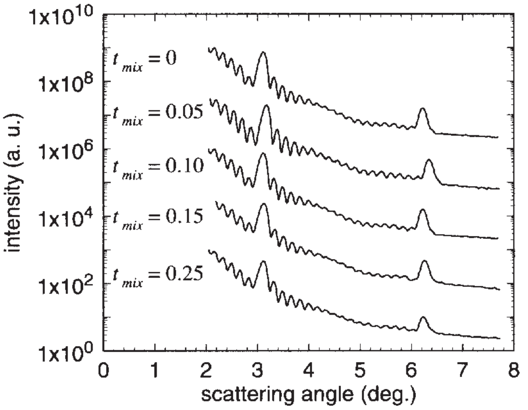

Fig. 2 Measured low angle x-ray diffraction patterns[18]. The large peaks at $2\theta = 3.1^\circ$ and 6.2° correspond to the Bragg diffraction for the superlattice period. For the better understanding, the data for the sample of t_{mix} = 0.15, 0.10, 0.05, and 0 nm are multiplied by $10^{1.5}$, 10^3, $10^{4.5}$ and 10^6, respectively.

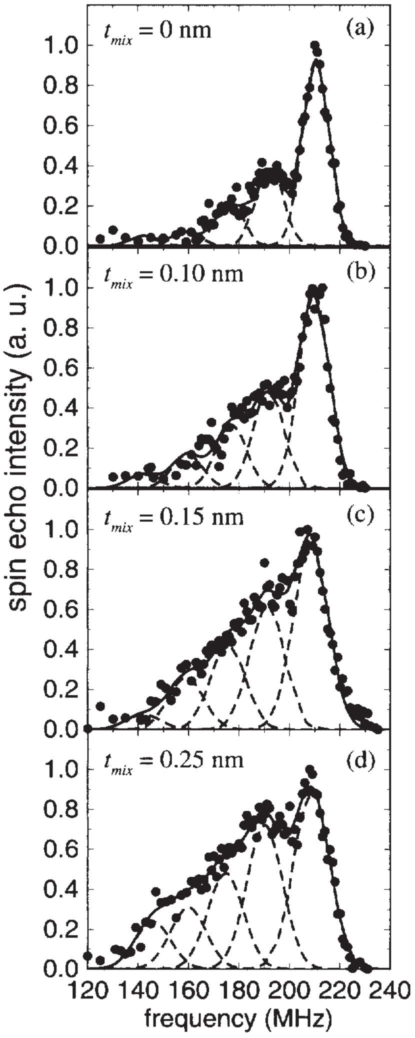

Fig. 3 Frequency spectra of spin-echo intensity of ^{59}Co[18]. Measured data (●) are fitted with 5 Gaussians (dashed lines). Solid lines indicate the summation of 5 Gaussians.

amount of the mixing of Co and Cu atoms increases with t_{mix}.

The chemical composition profile (CCP) and the ASRO parameters have been evaluated from the frequency spectrum. The calculation procedure is detailed in Ref. [18], and we report here only the result. Resulting CCP's shown in **Fig. 4** well reproduce the frequency spectra as indicated by solid lines in Fig. 3. The shape of the spectrum depends drastically upon CCP (parameters x_i). For example, there are significant change in the shape of the spectra for the samples of t_{mix} = 0, 0.10, and 0.15 nm (Fig. 3(a), (b) and (c)), while the differences in CCP's for these samples are not so large (Fig. 4(a), (b) and (c)). This indicates that the NMR has the power to detect the small differences in the CCP. Because of this high sensitivity of NMR to local composition, CCP's were determined within the errors indicated by bars in Fig. 4. For the sample of t_{mix} = 0 nm, the intermixing extends over 2 atomic layers near interface. The concentrations of Co in the first and second atomic layers from the interface are 84 and 97 %, respectively. With increasing t_{mix}, the amount of the intermixing increases. On the other hand, the ASRO parameters are almost zero in all atomic layers for all samples. In the case of $\alpha_i = 0$, Co and Cu atoms distribute randomly, while $\alpha_i < 0$ ($\alpha_i > 0$) corresponds to the ordering (segregation) of the Co and Cu atoms. Although, the shape of the spectrum is not so sensitive to the ASRO parameters (α_i) in the present case, their values of almost zero are enough reliable to preclude the strong ordering or segregation of the Co and Cu atoms. Therefore, atoms of Co and Cu are distributed randomly in the mixed regions.

The results for XRD and NMR are consistent with each other. Since the Co and Cu are randomly mixing at interfaces, the optical constants for x-ray will change from Co to Cu layer over a finite distance. On the other hand, the thickness of the mixing region is uniform in the sample as expected

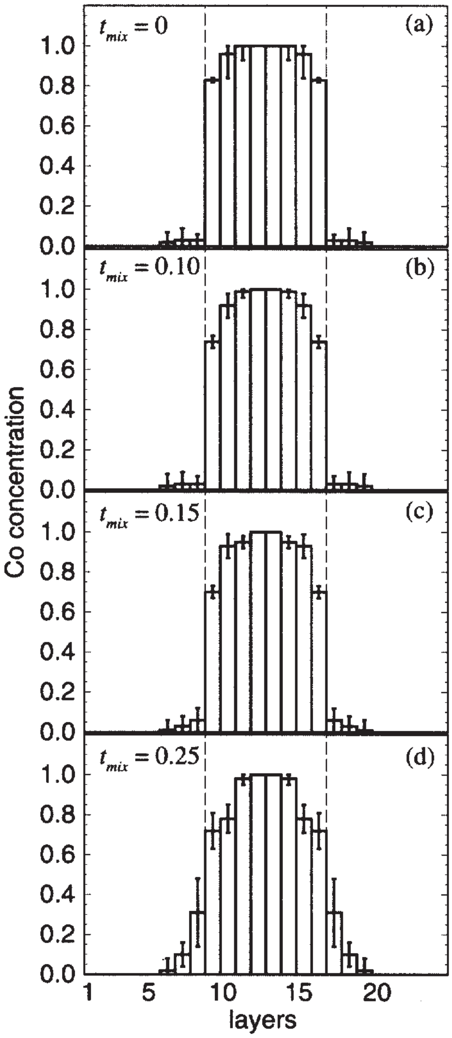

Fig. 4 Estimated chemical composition profile in one superlattice period[18]. Histogram shows the estimated Co concentration x_i in the ith atomic layer. Dashed lines indicate the boundaries of Co layer of 8 ML with ideal structure. Bars indicate the statistical error.

from XRD measurements. Therefore, no significant change in XRD pattern for the samples of different t_{mix} is observed. These facts confirm that our samples with different t_{mix} are only different in the distribution of Co atoms near interfaces, while the superlattice period, the thickness fluctuation and crystallinity remain unchanged. Consequently, we can control the atomic roughness of the interfaces in the Co/Cu superlattices by codeposition.

3.2 GMR[20]

Fig. 5 shows the MR curves measured at 5 K for the samples with different t_{mix}. The MR ratio is defined as $(\rho - \rho_F)/\rho_F$, where ρ is the resistivity in an arbitrary field and ρ_F is the saturation resistivity. In general, the resistivity of our samples decreases from the initial value with increasing magnetic field H and saturates at the value of ρ_F in a field larger than the saturation field H_s. After saturation, the resistivity has a peak near the coercive field. Since the value of the initial resistivity is larger than that of the peak one, the antiferromagnetic (AF) alignment of the magnetization of the Co layers is more perfect at the initial state than that in the field where the resistivity has the peak. The magnetization of all samples is zero at initial state, and the relationship between the resistivity and the square of the magnetization is linear at low temperatures. From the discussion in Ref. [20], this indicates that magnetic configuration of our samples is very close to the perfect AF alignment at the initial

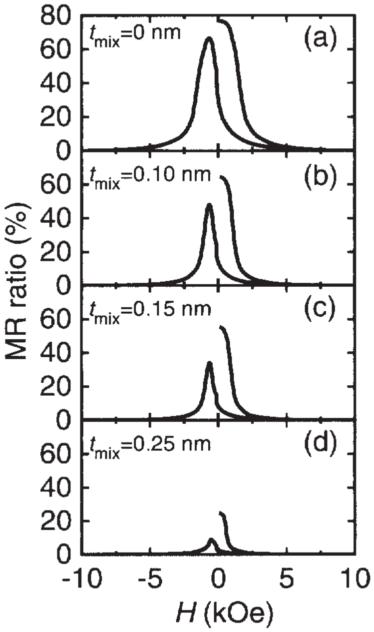

Fig. 5 The magnetoresistance curves measured at 5 K for samples with different interfacial roughness[20].

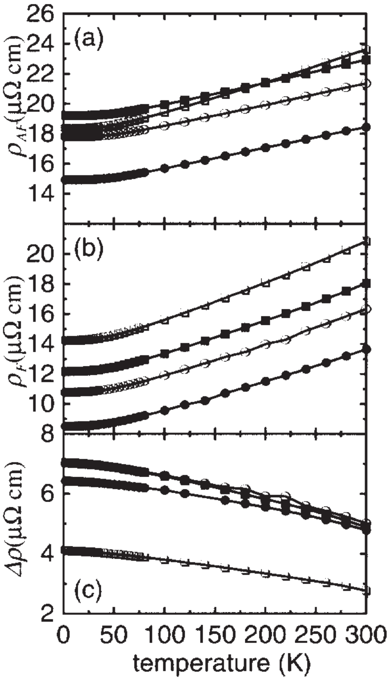

Fig. 6 Temperature dependence of (a) ρ_{AF}, (b) ρ_F, and (c) $\Delta\rho$ for the samples of t_{mix} = 0 (●), 0.10 (○), 0.15 (■), and 0.25 (□) nm[20]. Note that the vertical scale for (c) is different from the others. The lines indicate a guide for the eyes.

state. Then we denote the resistivity at the initial states as ρ_{AF} here. Furthermore, linear dependence of the resistivity on the square of the magnetization preclude the strong spin dependence in the scattering potential for both bulk and interfacial scattering.

We examined the effect of the interfacial roughness on the temperature dependence of the GMR with our attention on the initial resistivity ρ_{AF} and the saturation resistivity ρ_F. During the measurements of temperature dependence of ρ_{AF} and ρ_F, we can keep the magnetic configuration constant. **Fig. 6** shows the temperature dependence of ρ_{AF} and ρ_F together with that of $\Delta\rho = \rho_{AF} - \rho_F$ for the samples of various t_{mix}. With increasing temperature, both ρ_{AF} and ρ_F increase due to electron-phonon, electron-magnon, or other scattering processes. The residual resistivity of ρ_F increases with increasing t_{mix} due to the increase in interfacial scattering, though the difference in the temperature coefficient is small. Since the temperature coefficient of ρ_F is larger than that of ρ_{AF}, $\Delta\rho$ decreases with increasing temperature.

Fig. 7 and **8** show double logarithmic plots of $\rho_F(T) - \rho_F(2\ \mathrm{K})$ and $\Delta\rho(2\ \mathrm{K}) - \Delta\rho(T)$. At temperatures lower than 100 K, ρ_F closely approximates a T^2 power law. The temperature dependence of ρ_F changes to T^n ($n = 1 - 1.5$) over 100 K. On the other hand, $\Delta\rho$ changes linearly with $T^{3/2}$ over the whole measurement temperature range. Saito *et al.*[21] indicated that $\Delta\rho$ and the spontaneous magnetization showed a similar temperature dependence. In fact, the spontaneous magnetization of our samples also shows the $T^{3/2}$ dependence. However, the relationship between them is more complicated than a simple linear relation. The power laws for $\Delta\rho$ and ρ_F are independent of t_{mix}, although the residual $\Delta\rho$ and ρ_F change significantly due to the increase in interfacial roughness (see Fig. 6). This sug-

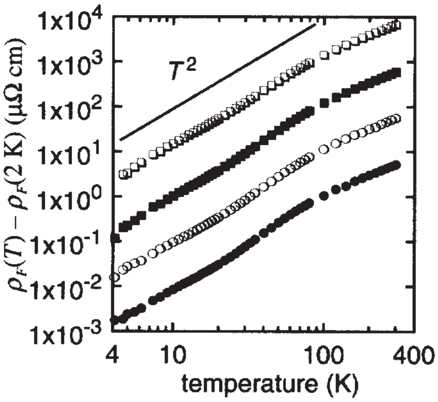

Fig. 7 Double logarithmic plot of $\rho_F(T)$–$\rho_F(2\ \mathrm{K})$ versus temperature for the samples of $t_{\mathrm{mix}} = 0$ (●), 0.10 (○), 0.15 (■), and 0.25 (□) nm[20]. For the better understanding, the data for the sample of $t_{\mathrm{mix}} = 0.10$, 0.15, and 0.25 nm are multiplied by 10, 10^2, and 10^3, respectively.

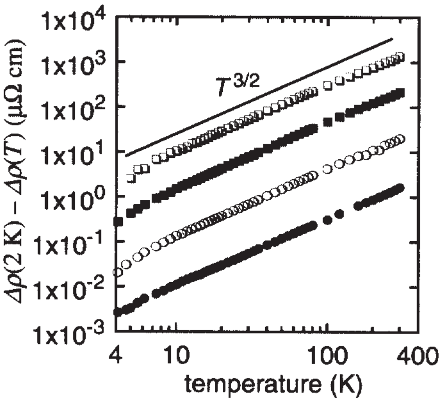

Fig. 8 Double logarithmic plot of $\Delta\rho(2\ \mathrm{K}) - \Delta\rho(T)$ versus temperature for the samples of $t_{\mathrm{mix}} = 0$ (●), 0.10 (○), 0.15 (■), and 0.25 (□) nm[20]. For the better understanding, the data for the sample of $t_{\mathrm{mix}} = 0.10$, 0.15, and 0.25 nm are multiplied by 10, 10^2, and 10^3, respectively.

gests that the interfacial scattering mainly contributes to the residual resistivity, while the temperature dependence mainly comes from the bulk scattering.

4. Discussion

In this section, we propose the simple model based on above experimental results to explain the t_{mix} dependence of the GMR at low temperature.

For the GMR in Co/Cu superlattices, scattering of *s* electrons to unfilled *d* bands is important. At the Fermi level, the majority spin band of Co and the conduction band of Cu have no *d*-like character, while the minority spin *d* band in Co has large density of states (DOS). Thus, the minority spin *d* states will be bound to the Co layers. On the other hand, *s* electrons near the Fermi level do not experience a large potential difference at any of the interfaces, since the *s* bands for Co and Cu are well aligned. Since the bulk and interfacial scattering can be attributed to the impurity scattering at low temperature as we mentioned above, we assume that the bulk and interfacial scattering potentials have the form of the Dirac delta function. Here, we do not assume any spin-dependence in the scattering potentials, since the resistivity depends linearly on the square of the magnetization. We have extended the resistor network theory[22] to take account of the bound *d* states using quantum Boltzmann equation. The details will be reserved for a separate publication[23], and we report here only the final result,

$$1/\rho_F = 1/\rho_\uparrow^F + 1/\rho_\downarrow^F \quad \cdots\cdots\cdots\cdots\cdots\cdots (1)$$

$$\rho_\uparrow^F = \frac{2\pi m_s}{\hbar N_s e^2}\left[g_s(E_F)\left(V_B^2\eta_B+\frac{4\varepsilon}{\lambda}\right)V_I^2\eta_I\right] \quad \cdot\cdot (2)$$

$$\rho_\downarrow^F = \frac{2\pi m_s}{\hbar N_s e^2}\left[g_s(E_F)(V_B^2\eta_B+\frac{4\varepsilon}{\lambda}V_I^2\eta_I) + g_d(E_F)\frac{t_M}{\lambda}(V_B^2\eta_B+\frac{4\varepsilon\phi_F}{\lambda}V_I^2\eta_I)\right] \quad \cdot\cdot (3)$$

$$2\rho_{AF} = \rho_\uparrow^{AF} = \rho_\downarrow^{AF} = \frac{2\pi m_s}{\hbar N_s e^2}\left[g_s(E_F)(V_B^2\eta_B+\frac{4\varepsilon}{\lambda}V_I^2\eta_I) + g_d(E_F)\frac{t_M}{2\lambda}(V_B^2\eta_B+\frac{4\varepsilon\phi_F}{\lambda}V_I^2\eta_I)\right] \quad \cdots\cdots\cdots\cdots\cdots\cdots (4)$$

m_s : effective mass of *s* electrons,
N_s : density of *s* electrons,
$g_s(E_F)$: DOS of *s* states at the Fermi energy of E_F,
$g_d(E_F)$: DOS of *d* states at the Fermi energy,
V_B : height of the scattering potential in the bulk,
V_I : height of the scattering potential at interfaces,
η_B : volume density of the bulk scatterers,
η_I : volume density of the interfacial scatterers,
ε : $\varepsilon = 2t_{\mathrm{mix}}$,
t_M : thickness of magnetic layer,
λ : superlattice period,
ϕ_F : square of the amplitude of *d* wave at interfaces.

In these equations, the terms with prefactor $g_s(E_F)$ and $g_d(E_F)$ come from the *s*-*s* and *s*-*d* scattering, respectively. The influence of the interfacial states are included explicitly by using ε (interfacial roughness) and ϕ_F (interfacial electronic states). In our model, the spin-dependent DOS of *d* states play an important role to arise the GMR.

Fig. 9 shows the t_{mix} dependence of the GMR measured at 5 K. Both ρ_{AF} and ρ_F increase with increasing t_{mix}, while the MR ratio decreases. It is clear that the interfacial scattering is crucial but less spin-dependent. We can estimate the value of $g_d(E_F)/g_s(E_F)$ at about 12 from the measured MR ratio of the sample of $t_{\mathrm{mix}} = 0$ nm, if we neglect the interfacial scattering [assuming $\varepsilon = 0$ nm in equations (1)-(4). This value of $g_d(E_F)/g_s(E_F)$ is close to the ratio of the calculated DOS at E_F in the majority and minority spin bands in bulk Co[24, 25]. The calculated resistivities and the MR ratio for the parameters of $t_M = 1$ nm, $\lambda = 3.2$ nm, $g_d(E_F)/g_s(E_F) = 12$ and $V_I^2\eta_I / V_B^2\eta_B = 5$ are also indicated by lines in Fig. 9. The calculated results are normalized at $t_{\mathrm{mix}} = 0$ as the calculated ρ_F to be equal to the measured one. It is clear that the behavior of ρ_F is insensitive to ϕ_F. The agreement between measured and calculated ρ_F is well when $V_I^2\eta_I / V_B^2\eta_B = 5.0\pm1.0$. It is reasonable that the density of the scattering centers is larger, or the scattering potential is stronger at interfaces than in bulk ($\eta_I > \eta_B$ or $V_I > V_B$). On the other hand, ρ_{AF} is sensitive to ϕ_F. Comparing the measured and the calculated results, $\phi_F \simeq 0.5$ is suitable for explaining the behavior of ρ_{AF} and the MR ratio for the samples of $t_{\mathrm{mix}} \leq 0.15$ nm. The approximation we made in Eqs. (1)-(4) will no longer hold, when t_{mix} becomes comparable with the period of the wave function of *d* states (see Ref. [23]). This affect ρ_{AF} much more than it does ρ_F, and may cause the deviation between the measured and calculated ρ_{AF} at $t_{\mathrm{mix}} = 0.25$ nm. The detailed numerical calculation will be necessary to discuss the GMR for the samples with such large roughness. The value of $\phi_F < 1$ indicates that amplitude of the *d* states is attenuated at interfaces, since the average value of square of the amplitude of *d* wave is about λ/t_M (> 1) in the magnetic layers. Thus, *d* states are strongly bound in magnetic layers.

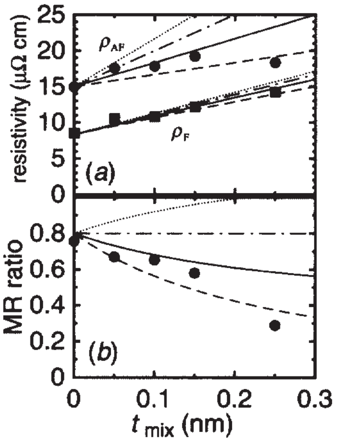

Fig. 9 Measured (symbols) and calculated (lines) resistivities (*a*) and the MR ratio (*b*)[23]. Measurement was performed at 5K. In (*a*), the measured ρ_{AF} (●) and ρ_F (■) correspond to the resistivities for antiferro- and ferromagnetic configurations, respectively. Parameters used in calculation are $t_M = 1$ nm, $\lambda = 3.2$ nm, $g_d(E_F)/g_s(E_F) = 12$ and $V_I^2\eta_I/V_B^2\eta_B = 5$. Lines indicate the results for $\phi_F = 0$ (dashed lines), $\phi_F = 0.5$ (solid lines), $\phi_F = 1.0$ (dashed-and-dotted lines) and $\phi_F = 1.5$ (dotted lines).

Our model agrees well with the experimental results. However, the contribution of the interfacial scattering to the resistivity of the sample of $t_{\mathrm{mix}} = 0$ nm remains unclear, although we neglect it in the above discussion. In fact, we have confirmed the existence of a small amount of interfacial mixing for the sample of $t_{\mathrm{mix}} = 0$ nm as we mentioned in Sec. **3.1**. The influence of the interfacial mixing can be also discussed by the layer thickness dependence of the resistivities. Thus, we focus our attention on the dependence of ρ_F, which is not influenced by the interlayer coupling between adjacent Co layers, on the thickness of the Co and Cu layers for the samples without intentionally mixed interfaces. As a result, ρ_F increases with increasing the Co layer thickness, while it decreases with increasing the Cu layer thickness. This indicates clearly that the resistivity of Co layers is larger than that of not only Cu layers but also the interfaces. This layer thickness dependence is reproduced only when ε is very small in Eqs. (1)-(4). Therefore, our assumption of $\varepsilon = 0$ for the sample of $t_{\mathrm{mix}} = 0$ nm is appropriate.

If superlattices have slightly rougher interfaces than that of our samples of $t_{\mathrm{mix}} = 0$ nm, the interfacial scattering will influence the GMR significantly depending on the interfacial electronic state. The interfacial electronic state should be sensitive to the combination of metals. Parkin[15] has reported that the MR ratio is enhanced by inserting very thin Co layers at the interfaces between Cu and NiFe layers. This can be interpreted in our model as the change in ϕ_F depending on materials. The virtual bound state indicated by Inoue and Maekawa[26] may also affect the magnitude of the GMR. However, the bulk *s*-*d* scattering will be the most important process to arise the GMR in *TM*/Cu superlattices, since a very large MR ratio is observed at least for our sample whose interfacial scattering is very small.

Consequently, the GMR in Co/Cu superlattices mainly comes from the spin-dependent bulk scattering due to spin-dependent DOS in the Co layers. The interfacial scattering due to interfacial roughness is less spin-dependent than the bulk scattering. This is understood in terms of the *d* states bound in the Co layers.

5. Conclusion

We have investigated the structure and the GMR of Co/Cu superlattices with artificially modified interfaces. We succeeded in preparing Co/Cu superlattices with well-controlled interfacial roughness. In these samples, only the atomic interfacial roughness has been modified, while the morphology and the crystallinity remain unchanged. The residual resistivity increases with increasing t_{mix}, while the temperature dependence of the GMR is independent of t_{mix}. The residual MR ratio decreases with increasing t_{mix}. The t_{mix} dependence of the residual GMR is well understood with the simple *s*-*d* scattering model. The GMR in Co/Cu superlattices mainly comes from the spin-dependent *s*-*d* scattering in the Co layers, and the interfacial scattering is less spin-dependent than bulk scattering. This is because of the attenuation of the wave function of *d* states at interfaces.

Acknowledgments

We acknowledge Professor Hiroshi Yasuoka and Atsushi Goto of ISSP, University of Tokyo for useful discussions and the support for NMR measurements. The skilled technical assistance provided by Atsuko Inoue is also appreciated.

References

[1] Baibich, M. N., Broto, J. M., Fert, A., Nguyen Van Dau, F., Petroff, F., Etienne, P., Creuzet, G., Friederich, A. and Chazelas, J. : Phys. Rev. Lett., **61**(1988), 2472

[2] Parkin, S. S. P., Bhadra, R. and Roche, K. P. : Phys. Rev. Lett., **66**(1991), 2152

[3] Mosca, D. H., Petroff, F., Fert, A., Schroeder, P. A., Pratt Jr., W. P. and Laloee, R. : J. Magn. Magn. Mater., **94**(1991), L1

[4] Levy, P. M., Zhang, S. and Fert, A. : Phys. Rev. Lett., **65**(1990), 1643

[5] Zhang, S. and Levy, P. M. : Phys. Rev. B, **43**(1991), 11048

[6] Inoue, J., Oguri, A. and Maekawa, S. : J. Phys. Soc. Jpn., **60**(1991), 376

[7] Xing, L., Chang, Y. C., Salamon, M. B., Frenkel, D. M., Shi, J. and Lu, J. P. : Phys. Rev. B, **48**(1993), 6728

[8] Xing, L. and Chang, Y. C. : Phys. Rev. B, **48**(1993), 4156

[9] Petroff, F., Barthélémy, A., Hamzić, A., Fert, A., Etienne, P., Lequien, S. and Creuzet, G. : J. Magn. Magn. Mater., **93**(1991), 95
[10] Fullerton, E. E., Kelly, D. M., Guimpel, J., Schuller, I. K. and Bruynseraede, Y. : Phys. Rev. Lett., **68**(1992), 859
[11] Hall, M. J., Hickey, B. J., Howson, M. A., Hammond, C., Walker, M. J., Wright, D. G., Greig, D. and Wiser, N. : J. Phys. Condens. Mater., **4**(1992), L495
[12] Saito, Y., Inomata, K., Goto, A. and Yasuoka, H. : J. Phys. Soc. Jpn., **62**(1993), 1450
[13] Speriosu, V. S., Nozieres, J. P., Gurney, B. A., Dieny, B., Huang, T. C. and Lefakis, H. : Phys. Rev. B, **47**(1993), 11579
[14] Suzuki, M. and Taga, Y. : J. Appl. Phys., **74**(1993), 4660
[15] Parkin, S. S. P. : Phys. Rev. Lett., **71**(1993), 1641
[16] Lenczowski, S. K. J., Gijs, M. A. M., Geisbers, J. B., van de Veerdonk, R. J. M. and de Jonge, W. J. M. : Phys. Rev. B, **50**(1994), 9982
[17] Yasuoka, H. : Metallic Superlattices, Ed by Shinjo, T. and Takada, T., (1987), 159, Elsevier, Amsterdam
[18] Suzuki, M., Taga, Y., Goto, A. and Yasuoka, H. : Phys. Rev. B, **50**(1994), 18580
[19] Suzuki, M., Taga, Y., Goto, A. and Yasuoka, H. : J. Magn. Magn. Mater., **126**(1993), 495
[20] Suzuki, M. and Taga, Y. : Phys. Rev. B, **52**(1995), 361
[21] Saito, Y., Inomata, K., Uji, S., Terashima, T. and Aoki, H. : J. Phys. Soc. Jpn., **63**(1994), 1263
[22] Edwards, D. M., Mathon, J. and Muniz, R. B. : IEEE Trans. Magn., **27**(1991), 3548
[23] Suzuki, M. and Taga, Y. : J. Phys. Condens. Mater., **7**(1995), 8497
[24] Ballinger, R. A. and Marshall, C. A. W. : J. Phys. F, **3**(1973), 735
[25] Mehta-Ajmani, M., Batra, I. P., Lafon, E. E. and Fadley, C. S. : J. Phys. C, **13**(1980), 2807
[26] Inoue, J. and Maekawa, S. : J. Phys. Soc. Jpn., **61**(1992), 1149

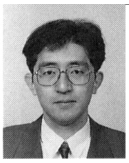

Motofumi Suzuki was born in 1963. He received M. E. degree in engineering science from Kyoto University in 1988. He belongs to the Thin Film Laboratory, where he works on the transport, magnetic, and optical properties of nano-structured materials. He is a member of the Physical Society of Japan and the American Physical Society.

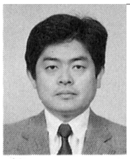

Takeshi Ohwaki was born in 1956. He received M. E. and D. E. degree in crystalline materials science in 1981 and 1994, respectively, both from Nagoya University. He belongs to the Thin Film Laboratory, where he works on thin films and surface and interface physics. He is a member of the Japan Society of Applied Physics and Chemical Society of Japan.

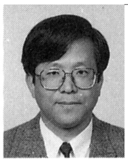

Yasunori Taga joined Toyota Central R & D Labs in 1970 after graduation from Nagoya Institute of Technology. He received Dr. Eng. in Materials Science from Osaka University in 1979. He became a manager of Electronics Device Division, where he works on thin film and surface and interface physics. He is a member of American Institute of Physics, American Vacuum Society, Materials Research Society, IEEE , and The Japan Society of Applied Physics.